

Seismological Research Letters
**Analysis of the 2005-2015 Earthquake Sequence in Northern Iran Using the Visibility
Graph Method**
--Manuscript Draft--

Manuscript Number:	
Full Title:	Analysis of the 2005-2015 Earthquake Sequence in Northern Iran Using the Visibility Graph Method
Article Type:	Article - Regular Section
Corresponding Author:	Ricardo Taborda, Ph.D. University of Memphis Memphis, TN UNITED STATES
Corresponding Author Secondary Information:	
Corresponding Author's Institution:	University of Memphis
Corresponding Author's Secondary Institution:	
First Author:	Naeem Khoshnevis
First Author Secondary Information:	
Order of Authors:	Naeem Khoshnevis Ricardo Taborda, Ph.D. Shima Azizzadeh-Roodpish Luciano Telesca, Ph.D.
Order of Authors Secondary Information:	
Manuscript Region of Origin:	IRAN (ISLAMIC REPUBLIC OF)
Suggested Reviewers:	Alejandro Ramirez-Rojas Prof, Universidad Autonoma Metropolitana alexramro@gmail.com Has published papers on this subject before. Chien-Chih Chen Prof, National Central University, Taoyuan, Taiwan chencc@earth.ncu.edu.tw Published related papers on changes of seismicity parameters in earthquake sequences Morgan Moschetti US Geological Survey mmoschetti@usgs.gov has research experience in seismicity and seismic hazard analysis Panayiotis A Varotsos Professor, University of Athens pvaro@otenet.gr Has looked at the problem of statistical properties of earthquakes in time Page Morgan US Geological Survey mpage@usgs.gov Bright young researcher... might find this of interest to review
Opposed Reviewers:	



COPYRIGHT/COLOR--CHARGES FORM

FILL OUT, SCAN, AND SUBMIT THIS FORM ONLINE WHEN SUBMITTING YOUR PAPER

Manuscript Number: SRL-D- _____ [leave blank for new submissions]

Title: Analysis of the 2005-2015 Earthquake Sequence in Northern Iran Using the Visibility Graph Method

Authors: Naeem Khoshnevis, Ricardo Taborda, Shima Azizzadeh-Roodpish, and Luciano Telesca

COPYRIGHT

In accordance with Public Law 94-533, copyright to the article listed above is hereby transferred to the Seismological Society of America (for U.S. Government employees, to the extent transferable) effective if and when the article is accepted for publication in *Seismological Research Letters*. The authors reserve the right to use all or part of the article in future works of their own. In addition, the authors affirm that the article has not been copyrighted and that it is not being submitted for publication elsewhere.

To be signed by at least one author (who agrees to inform the others, if any) or, in case of "work made for hire," by the employer.

Ricardo Taborda, Asst. Professor

26 Aug 2016

Authorized

Signature for Copyright

Print Name (and title, if not author)

Date

PUBLICATION CHARGES

Page charges: The Seismological Society of America requests that institutions supporting research share the cost of publicizing results of that research. The Editor has discretion to waive publication charges for authors who do not have institutional support. In addition to regular publication charges there is a nominal fee for publishing electronic supplements. **Some article types do not incur page charges.** Current rates and information about are available at <http://www.seismosoc.org/publications/journal-publication-charges/>

Color options: Color figures can be published (1) in color both in the online journal and in the printed journal, or (2) in color online and in grayscale in print. Online color is free; authors will be charged for color in print. You must choose one option for all of the color figures within a paper; that is, you cannot choose option (1) for one color figure and option (2) for another color figure. You cannot submit two versions of the same figure, one for color and one for grayscale. You are responsible for ensuring that color figures are understandable when converted to gray scale, and that text references and captions are appropriate for both online and print versions. Color figures must be submitted before the paper is accepted for publication. See additional information at <http://www.seismosoc.org/publications/srl/srl-authorsinfo/>

Will publication charges be paid? Check only one:

BOTH PAGE CHARGES AND COLOR CHARGES WILL BE PAID. All color figures for this paper will be color both online and in print. This option requires full payment of publication & color charges.

ONLY PAGE CHARGES WILL BE PAID. All figures for this paper will be grayscale in print. Color figures, if any, will be color online.

REQUEST A REDUCTION IN PAGE CHARGES. Send a letter of request and explanation to the Editor-in-Chief at SRL@seismosoc.org. Color figures, if any, will be color online but grayscale in print.

ONLY COLOR CHARGES WILL BE PAID. The article is exempt from page charges, but you wish to print color figures. This option is available only for select SRL article types that are exempt from page charges and requires full payment of color charges.

PUBLICATION CHARGES DO NOT APPLY. The article type doesn't incur page charges and there are no color figures.

Send Invoice to (required for ALL SRL submissions) :

Ricardo Taborda, 3890 Central Ave., Memphis, TN 38152

If your paper is accepted for publication, SSA will require you to fill out and submit an online billing/offprint-order form.

¹ ***Analysis of the 2005–2015 Earthquake Sequence in***

² ***Northern Iran Using the Visibility Graph Method***

³ **Naeem Khoshnevis,^{1,*} Ricardo Taborda^{1,2} Shima Azizzadeh-Roodpish,^{1,2} and**

⁴ **Luciano Telesca³**

⁵ 1. Center for Earthquake Research and Information
⁶ The University of Memphis, Memphis, TN 38152, U.S.A.

⁷ 2. Department of Civil Engineering
⁸ The University of Memphis, Memphis, TN 38152, U.S.A.

⁹ 3. Institute of Methodologies for Environmental Analysis
¹⁰ National Research Council, Tito, Italy

¹¹ *. Corresponding author
¹² Email: nkhshnvs@memphis.edu

¹³ August 26, 2016

14 **ABSTRACT**

15 We present an analysis of the seismicity of northern Iran in the period between 2005 and 2015 using a recently introduced method
16 based on concepts of graph theory. The method relies on the inter-event visibility defined in terms of a connectivity degree param-
17 eter, k , which is correlated with the earthquake magnitude, M . Previous studies show that the slope of the k - M correlation also
18 observes a relationship with the b -value from the Gutenberg-Richter law, thus rendering the graph analysis useful to examine the
19 seismicity of a region. In addition, other topological properties of the network and dynamic properties of the magnitude-time series
20 exhibit characteristics that seem to be associated with the occurrence of earthquakes, offering the possibility of correlating seismic-
21 ity parameters with time. We apply this approach to the case of the seismicity of northern Iran, using an earthquake catalog for
22 the tectonic seismic regions of Azerbaijan, Alborz, and Kopeh Dagh. We use results drawn for this region with the visibility graph
23 approach in combination with results from other similar studies to further improve the universal relationship between the slope
24 of k - M and b -value, and show that the visibility graph approach can be considered as a valid alternative for analyzing regional
25 seismicity properties and earthquake sequences.

26

27 INTRODUCTION

28 In a relatively recent study, [Lacasa et al. \(2008\)](#) introduced a simple and computationally inexpensive approach to convert time-
29 series into a particular kind of mathematical graphs known as visibility graphs. In this approach, the connection between the nodes
30 in a network—here understood as events in a time series—is based on the visibility of each node or event with respect to other
31 previous and later events in a time sequence. Over the last decade, this method has been found to be applicable to multiple fields,
32 including economics, medicine, and geophysics (e.g., [Yang et al., 2009](#); [Elsner et al., 2009](#); [Telesca et al., 2012](#); [Wang et al., 2012](#);
33 [Long, 2013](#)).

34 For the particular case of seismological applications, previous studies have proposed to consider the nodes in the graph to
35 be the earthquakes in a given time series of events, and analyzed the properties of the graph with respect to traditional seismicity
36 parameters. The analysis of seismic sequences through the visibility graph approach for various tectonic seismic regions has proven
37 to be a valid alternative to studying magnitude time series. [Telesca and Lovallo \(2012\)](#), for instance, studied the seismicity of Italy
38 between the years 2005 and 2010 using the visibility graph method. Applying different threshold magnitudes to construct the graph
39 and observing the collapsing effect of all distribution degrees, they observed that the properties of the visibility graph seemed to
40 depend only on the magnitude values, and not on the threshold magnitude used in the analysis.

41 Subsequently, [Telesca et al. \(2013\)](#) studied the seismicity of the Mexican subduction zone through the visibility graph approach
42 and found that the properties of the graph were correlated to the seismic *b*-value in the Gutenberg-Richter law ([Gutenberg and](#)
43 [Richter, 1944](#)). In particular, [Telesca et al. \(2013\)](#) extracted the characteristics of the visibility graph for five different tectonic
44 seismic regions in the subduction zone and found that the slope in the linear relationship between earthquake magnitude, *M*, and
45 the inter-event visibility in the graph defined as the connectivity degree parameter, *k*, was correlated with the *b*-value.

46 In a similar article, [Telesca et al. \(2014b\)](#) studied the seismicity of the 2002–2011 Pannonian region using the visibility graph
47 method for two sub-catalogs of shallow and deep earthquakes. They extracted the visibility graph characteristics for each group of
48 events and confirmed that there was a close correlation between the Gutenberg-Richter *b*-value and the slope of the *k*-*M* relationship
49 obtained from the visibility graph. According to [Telesca et al. \(2014b\)](#), the high linear correlation coefficient value (close to 1.0)
50 between the *b*-value and the *k*-*M* slope indicates that this relationship exhibits a nearly universal character. This observation was
51 reinforced experimentally by [Telesca et al. \(2014a\)](#), who investigated the behavior of a mechanical stick-slip system with different
52 asperities (sandpaper of different grades). After collecting data for different experiments emulating young and mature faults,
53 [Telesca et al. \(2014a\)](#) found again that the *b*-value was linearly correlated with the *k*-*M* slope derived from the visibility graph of
54 the experimental events.

55 More recently, [Telesca et al. \(2016\)](#) used the visibility graph method to gain insight about the timespan between earthquakes.
56 The authors defined the parameter $\langle T_c \rangle$ as the window mean interval connectivity time, which provides information about the
57 average of all the time intervals between visible events. Applying this concept to the 2003–2012 earthquake sequence in Kachchh,
58 western India, [Telesca et al. \(2016\)](#) found that the variation of $\langle T_c \rangle$ in time exhibited a plausible relationship with the occurrence

59 of earthquakes. In particular, they observed that the value of $\langle T_c \rangle$ decreases significantly before the largest shock in the Kachchh
60 catalog.

61 In this article we use the visibility graph method to analyze the seismicity of northern Iran from 2005 to 2015. We focus our
62 analysis on these years because in a previous study we observed that the latest decade of seismic records in the region offered
63 the most complete catalog of events (e.g. [Khoshnevis et al., 2016](#)). Upon a brief review of the basic concepts of the method and
64 its applications, we describe the seismicity of northern Iran considering three dominant seismic regions: Azerbaijan, Alborz, and
65 Kopeh Dagh. These are regional areas of considerable ground shaking activity, with average seismic rates varying between about
66 0.17 and 3.25 events per year (e.g., [Nemati, 2015](#)). The considerable amount of earthquakes registered in a 10-year period facilitates
67 the analysis done with the visibility graph approach within what would otherwise be considered a relatively short period of time,
68 and serves as a good case study to test the capabilities of the method. We first summarize the dataset, including a description of
69 the seismic catalog and its completeness based on a recent work on the seismicity of the region ([Khoshnevis et al., 2016](#)). We then
70 present results obtained for the region regarding the relationship between the the graph's k - M slope and the seismicity b -value for
71 the three seismic areas, analyze the sensitivity of the catalogs to the number of events and the threshold magnitude, and present
72 results for the variation of $\langle T_c \rangle$ through time.

73 METHODOLOGY

74 Discrete mathematics and computer science often deal with different types of data abstractions and structures such as sets, trees,
75 and graphs, where concepts like nodes and links are used to describe the topology of a collection of objects and manipulate their
76 data (e.g., [Skiena, 2008](#)). In graphs, the data—sometimes also referred to as the payload—resides at the vertices or nodes who
77 are connected through links or edges, which may or may not have an associated direction. A visibility graph is a special type of
78 undirected graphs in which the links are straight lines connecting intervisible nodes; that is, straight lines that do not overlap any
79 obstacle while connecting nodes that can see each other in a physical space ([Lozano-Pérez and Wesley, 1979](#)). Visibility graphs
80 have been mostly used in robotics for navigation path planning (e.g., [Huang and Chung, 2004](#); [Oommen et al., 1987](#)) but have
81 also seen applications in other fields including urban studies, interior architecture, medicine and geosciences (e.g., [Raman, 2010](#);
82 [Ahmadlou et al., 2010](#); [Varoudis and Psarra, 2014](#); [Phillips et al., 2015](#)).

83 In a relatively recent study, [Lacasa et al. \(2008\)](#) applied the concepts of visibility graphs to the representation and analysis of
84 time series. Multiple applications have been found to this idea in fields such as economics ([Yang et al., 2009](#); [Wang et al., 2012](#)) and
85 climate studies ([Elsner et al., 2009](#)). In this study, we are particularly interested in the application of visibility graphs to the analysis
86 of seismic sequences ([Telesca and Lovallo, 2012](#)). In this case, the nodes in the visibility graphs are considered to be seismic events
87 distributed over time. For any seismic time series, two characteristics are attributed to each event: (a) its occurrence time, and (b)
88 the value associated to the event, here considered as the magnitude. The obstacles in the time space are the vertical lines (or sticks)
89 between the time axis and the magnitude of the event in a time-magnitude series. Two events are in connection, or visible to each
90 other, whenever no other event interrupts their linear connection.

91 In mathematical form, events i and j are visible to each other if they satisfy the inequality

92

$$\frac{y_i - y_p}{t_p - t_i} > \frac{y_i - y_j}{t_j - t_i}, \quad (1)$$

93 where y is the value associated with the event and t is the time of the event. The index p indicates any event occurring between events
94 i and j . It follows from this that the visibility graph generated from a time series holds the following conditions. Connectivity:
95 each event is visible to the two events to its immediate right and left sides, if there is any. Directivity: the graph is considered
96 undirected by definition; that is, the algorithm explaining the connections between events is developed without defining a direction
97 for the links between the events. And invariance: scaling or time-shifting the series does not change the resulting visibility graph,
98 provided the transformation is done under affine conditions (Lacasa et al., 2008).

99 Figure 1 shows an example of a visibility graph for a portion of one of the magnitude-time series to be considered later in this
100 study. For each event i we compute the connectivity degree, k , which is the sum of the connections to all other events j visible
101 by the i th event. Events are often categorized in small magnitude bins with $\Delta M = 0.1$ and we plot the connectivity degree as a
102 function of the bin magnitude. Note that two earthquakes with the same magnitude can have different k values, which ultimately
103 depend on the occurrence time of the event and whether the time-neighboring events are of a larger or smaller magnitude.

104 [Figure 1 about here.]

105 Plotting k against magnitude results on a scattered set of points which have been shown to be acceptably represented by a linear
106 regression. We referred to this correlation as the k - M relationship. More important, the slope of the k - M relationship also shows
107 a linear regression with the seismicity b -value of the seismic zone under consideration. This is also true for a universal sample
108 of k - M slopes and b values (Telesca et al., 2013, 2014b). Telesca et al. (2014b) also observed that it was reasonable to draw a
109 relationship between the distribution of the events when considering whether these were connected (visible to each other) or not,
110 and time. Let T_c be the interval connectivity time, which is nothing but the time difference between two inter-visible events (see
111 Fig. 1); and $\langle T_c^e \rangle$ be the average of all T_c values computed for event e ; then it is possible to compute the visibility graph mean
112 interval connectivity time $\langle T_c \rangle$, which is the mean value of all $\langle T_c^e \rangle$ in a given time sequence of events.

113 Because $\langle T_c \rangle$ can be obtained for any sub-graph within a larger graph, that is, for any time window in a larger magnitude-
114 time series of events, then it is possible to investigate the evolution of $\langle T_c \rangle$ (and that of the k - M slope and the b -value) for
115 a moving window—with a constant number of events—sliding along the magnitude-time series. When doing so, Telesca et al.
116 (2016) suggested to associate the values of each sub-sequence with the last event in the sub-sequence. Following this approach,
117 Telesca et al. (2016) found that the variation of $\langle T_c \rangle$ over time exhibited a possible relationship with the occurrence of earthquakes.
118 This and the aforementioned relationship between the k - M slope and the b -value are aspects we explore next for our region and
119 years-interval of interest.

120 SEISMICITY OF NORTHERN IRAN

121 We are interested in applying the visibility graph method to analyze the seismicity of northern Iran. This region is part of the
122 Iranian plateau, on the Himalayan-Alpine seismic belt. It is confined by the relative movements between the Arabian, Eurasian,

eastern Asia-Minor, and Indian plates; and has a long history of large magnitude ($M > 7$) earthquakes that are well documented dating back to the eight century (e.g., [Berberian, 1981](#)). According to the tectonic settings and geologic provinces of the plateau, the seismic activity in Iran has been categorized into different seismic zones. These vary between four to nine major seismic zones, in the more traditional models (e.g., [Stocklin, 1968](#); [Takin, 1972](#); [Berberian and Arshadi, 1976](#)), up to twenty to twenty-three seismotectonic provinces in the most elaborate ones (e.g., [Nowroozi, 1976](#); [Tavakoli and Ghafory-Ashtiani, 1999](#)). We adopt the model proposed by [Mirzaei et al. \(1998\)](#) with modifications introduced by [Karimiparidari et al. \(2013\)](#). In it, Iran is divided into six seismic regions: Azerbaijan, Alborz, Kopeh Dagh, Zagros, Central-East Iran, and Makran. Our focus, however, is on the northern part of Iran, for which we define a region of interest between longitudes 43.5°E and 61.5°E , and latitudes 34°N and 40°N , as shown in Fig. 2. Although this region encloses part of the Zagros and Central-East seismic zones, we concentrate in the analysis of the seismicity of Azerbaijan, Alborz and Kopeh Dagh.

[Figure 2 about here.]

Northern Iran houses about 41 percent (32 million) of the total population of the country, and has suffered devastating earthquakes in the past (e.g., [Mehrain, 1990](#); [Ghafory-Ashtiani, 1999](#); [Razzaghi and Ghafory-Ashtiani, 2012](#)). At the northwest, the seismic zone of Azerbaijan is strongly controlled by the North Tabriz Fault system in the vicinity of the city of Tabriz, shown in Fig. 2. Historical accounts document the occurrence of strong $M > 6$ earthquakes in this region as far back as the ninth century ([Berberian and Yeats, 1999](#)), and a few $M > 7$ earthquakes in 1042, 1721 and 1780 ([Jones, 1834](#)). More recently, this region was struck by the $M_w 6.1$ 1997 Ardabil earthquake near the city of Ardabil and the $M_w 6.4$ 2012 Tabriz earthquake northeast of the city of Tabriz. These earthquakes caused extensive damage and took the lives of more than 1,500 people.

The seismicity in the north-central region of Alborz is dominated by multiple fault systems, including the Talesh, Rubdar, North Alborz, and North Tehran faults, which also have a history of producing strong ground shaking. According to [Ambraseys and Melville \(1982\)](#), Tehran was devastated by severe $M > 7$ earthquakes in 743, 958, 1177, 1665, and 1830. This region has also seen some significant recent seismic activity ([Berberian and Yeats, 1999](#)), including the $M_w 7.4$ 1990 Manjil-Rudbar earthquake, which caused numerous deaths and damage to the region in the south Caspian depression, south from the city of Rasht and northwest from Tehran.

Last, there is the Kopeh Dagh seismic zone to the east and northeast. This region is dominated by the Main Kopeh Dagh Fault system, which exhibits active tectonic displacements along a distance of more than 500 km ([Trifonov, 1978](#)). This fault is responsible for the $M_w 7.3$ 1948 earthquake, which struck the capital city of Ashgabat in Turkmenistan and destroyed more than 30 villages in Iran. Historically, the Kopeh Dagh seismic zone is also responsible for the $M_s 7.1$ earthquake in 10 A.D. ([Berberian and Yeats, 2001](#)) near Ashgabat, and two significant earthquakes in 1209 and 1405 at the boundary between the Neyshabur and Binalud faults near the city of Mashhad ([Berberian and Yeats, 1999](#)).

[Figure 3 about here.]

It follows from this description that the region of interest is one of significant seismic activity, which goes back centuries. We are, however, interested in the most recent instrumental seismicity. In particular, we focus on events recorded in the last decade,

156 between January 2005 and December 2015. We focus our analysis on this magnitude-time sequence period because in a previous
157 study we observed that the latest decade of seismic records in northern Iran offered the most complete dataset of recorded events,
158 especially for the case of small $M < 4$ earthquakes (e.g. [Khoshnevis et al., 2016](#)).

159 We compiled a catalog of all recorded earthquakes using data downloaded from the International Institute of Earthquake
160 Engineering and Seismology, IIEES (see the Data and Resources section). The obtained dataset contained a mixture of earthquake
161 magnitude scales, including: moment, M_w ; local, M_L ; body wave, m_b ; surface wave, M_s ; and duration M_D magnitudes. We
162 converted all earthquakes to moment magnitude, M_w . Magnitudes in the M_L , m_b , and M_s scales were converted using the
163 relationships defined in [Zare et al. \(2014\)](#), whereas M_D magnitudes were converted using the empirical relationship proposed by
164 [Deniz and Yucemen \(2010\)](#).

165 Foreshocks and aftershocks were removed from the catalog following a Poissonian occurrence model using the declustering
166 method of [Gardner and Knopoff \(1974\)](#), in a manner consistent with previous catalog compilations available for the region (e.g.,
167 [Zare et al., 2014](#)). Upon declustering, we divide the catalog into three sub-catalogs, each for one of the seismic zones under
168 consideration. Fig. 3 shows the epicenter location of declustered instrumental earthquakes for the three seismic zones of interest.

169 We then proceeded to determine the minimum magnitude of completeness, M_c , for each region's sub-catalog. The value of
170 M_c is often determined using simple numerical analyses in combination with data inspection. Two common approaches are the
171 maximum curvature (MAXC) and the goodness-of-fit test (GFT) methods ([Wiemer, 2001](#)). We use the GFT method as introduced
172 by [Wiemer and Wyss \(2000\)](#). In this method, the completeness magnitude is obtained such that the catalog satisfies—at a certain
173 acceptance threshold—the Gutenberg-Richter power law, given an extended dataset of events. This extended dataset is composed
174 of predicted and observed events, where the predicted events are generated based on a trial minimum magnitude. The process is
175 repeated for increasing values of the reference minimum magnitude until finding a desirable fit with the power law. [Wiemer and](#)
176 [Wyss \(2000\)](#) suggests a goodness of fit of 90% as an acceptable threshold to select M_c . However, not all frequency-magnitude
177 distributions reach the 90% mark, in which case M_c can be selected by inspection.

178 Figure 4 shows the goodness-of-fit values for the three seismic zones. We indicate the selected value of M_c for each region in
179 the figure. We also obtained the b -value in the Gutenberg-Richter law for each region following the maximum likelihood estimation
180 ([Aki, 1965](#)):

$$181 b = \frac{\log_{10}(e)}{\bar{M} - M_{min}}, \quad (2)$$

182 where e is the mathematical constant or Euler's number, \bar{M} is the average magnitude, and M_{min} is the minimum magnitude in
183 the sample. Here, the value of M_{min} is taken as the minimum completeness magnitude M_c obtained or selected for each region's
184 sub-catalog. Table 1 shows the corresponding values of M_c and b .

185 [Figure 4 about here.]

186 [Table 1 about here.]

187 [Figure 5 about here.]

In addition to using M_c to determine the b -value for each sub-catalog, we also use M_c as the threshold for limiting the minimum magnitude to be considered in the construction of the visibility graph of each region. The resulting number of events for each region is included in Table 1. Figure 5 shows the final time-magnitude sequences for Azerbaijan, Alborz and Kopeh Dagh. Note that in the case of Alborz and Kopeh Dagh, we consider events in the declustered catalog down to $M_w \geq 2.6$, whereas in the case of Azerbaijan all events are $M_w \geq 3.5$.

RESULTS

We generate the visibility graph for each sub-region of interest using the time-magnitude sequences shown in Fig. 5. The number of nodes in each graph is the same as the (declustered) number of events shown in Table 1, and the links between inter-visible events are established following the condition in equation (1), as in the example shown in Fig. 1. (We do not include a visualization of the complete sequence graphs because the links are so many, it is only practical to visualize the graphs of short sequences.) We then collect information about the number of inter-visibility links associated with each event (connectivity degree, k) and categorize the events in magnitude bins of size $\Delta M = 0.1$, as mentioned in the Methodology section. Figure 6 shows the scattered distribution of events in the magnitude-connectivity degree plane for each sub-region. The figure shows that, in general, the value of k increases with M_w . Figure 6 also shows the results of obtaining linear k - M regressions for each dataset and the values of the k - M slopes for the three seismic zones.

[Figure 6 about here.]

Next, we examine the relationship between the b -values from Table 1 and the k - M slope values shown in Fig. 6. Figure 7 shows the scattered results for k - M slope versus b -value for the three tectonic seismic regions in northern Iran along with the data-points obtained for the analysis of the magnitude-time sequences of the Mexican subduction zone (Telesca et al., 2013) and the Pannonian seismic zone (Telesca et al., 2014b), as well as other experimental results (Telesca et al., 2014a). Figure 7 also includes the results of different linear regressions between the b -value and the k - M slope. Each regression reflects the addition of new data-points from different studies. Note that the regression improves as new data-points are added, which is indicated by the correlation coefficient R , also included in the figure. The correlation fitting various regional seismic data was previously pointed out by Telesca et al. (2014b).

According to these results, a universal relationship between the b -value and the k - M slope (m) can be expressed as:

$$b = 0.078 + 0.085m. \quad (3)$$

[Figure 7 about here.]

Another aspect of interest is the stability of the data points themselves. Note that as presented in Fig. 7, the analysis of the sequences shown in Fig. 5 only contribute one data point per region of interest. Furthermore, each data-point comes from sequences that vary significantly in terms of the number of events and seismic parameters (see Table 1).

218 Telesca et al. (2013) observed that the value of the k - M slope is not particularly sensitive to the sample size in the sequence—
219 at least not when considering sufficiently large sequences. On the other hand, as we will see below, if the sequence window is
220 sufficiently small, then the k - M slope value shows a relative dependence on time and thus provides insight about the variation of
221 the seismicity as the sequence progresses. Note also that the threshold value of M_c is significantly smaller for Azerbaijan than for
222 Alborz or Kopeh Dagh. This is due in part to the fact that the latter two zones were more seismically active in the time period
223 under consideration. However, according to Telesca and Lovallo (2012), the threshold magnitude has a minor effect in the graph
224 parameters.

225 To further explore the sensitivity of the graph properties to the number of events in each catalog and the value of the minimum
226 magnitude, we randomly picked a significant number of sub-sequences from within the initial catalog compiled for each region,
227 and repeated the analysis for each sub-sequence. In total, for each region, we extracted 200 new sub-sequences from the initial
228 (pre-declustering) catalog. The number of events in each sub-sequence was varied randomly but chosen to be large enough to
229 represent the seismic characteristics of each region. In particular, the minimum size of each sub-sequence was set to be $n \geq 150$,
230 and the maximum size in the sequence was set to be as large as the original catalog (pre-declustering; see Table 1). We forced
231 the random sub-sequences to progress positively in time without altering the natural occurrence of events. In other words, we
232 randomly determined the initial event and the sub-sequence size (number of events to be considered), and then picked that number
233 of events following the initial earthquake in the sub-sequence. Next, we determined the value of M_c and b as previously done for
234 the complete catalogs, created the graph for all events with $M \geq M_c$, and extracted the connectivity degree of the events in each
235 sub-sequence.

236 [Figure 8 about here.]

237 Figure 8a shows scattered points for all the individual k - M slope and b -value pairs for all the sub-sequences that were randomly
238 picked from the initial catalogs of each region in northern Iran (small symbols). Figures 8b and 8c show the variability of the k - M
239 slope and b -value, respectively. These latter figures show the mean values of each parameter for all the random sub-sequences and
240 the amplitudes of ± 1 standard deviation, as well as the coefficients of variation (in percentage). Figure 8a also includes the data
241 points corresponding to the complete catalogs (large solid symbols); the points corresponding to the mean values of the k - M slope
242 and b , from Figs. 8b and 8c (large hollow symbols); and the universal linear regression from equation (3) (thick line), as well as the
243 linear regressions for northern Iran when using the complete catalogs (dashed thin line) and the random sub-catalogs (continuous
244 thin line).

245 The comparison between the mean values of the random sequences analysis versus the complete catalogs presented in Fig. 8
246 indicates that there exists only a small bias, which is well within the standard deviation of the different value samples. We note that
247 the values of the k - M slope are slightly smaller when obtained with the random sequence analysis, whereas the b values seem more
248 stable. The comparisons of the regressions, however, indicate that the analysis of the random sub-catalogs leads to a result more in

line with the universal results obtained when considering multiple seismic zones. The linear regression of the random sub-catalogs yields the following equation:

$$b = 0.080 + 0.093m . \quad (4)$$

Note that equations (3) and (4) have similar intercepts with the b -value axis, and only slightly different slope constants. In this particular case, the analysis for northern Iran leads to a relationship in which the b -value increases more rapidly with m than in the case of the regression obtained for the universal data. The similarity between the two equations, however, is a positive sign of the stability of the method.

[Figure 9 about here.]

We now investigate the relationship of the parameters obtained through the visibility graph analysis with time. Here, the visibility graph analysis is done by windows of equal number of events moving in time across the catalog sequence. The number of events in the window is kept fixed independently of the time between them, and the results are associated with the last event in the window. In this case, we are interested in using a small number of events to capture the relevance of each new event as the window moves in time. We tried different numbers and finally chose 20 events as the moving window sequence size. This selection was also convenient given the smaller total number of declustered events in the catalog of Azerbaijan. When we tested larger number of events, we found that we could not properly observe the changes in the different parameters with time. On the other hand, when we used smaller sequence sizes, the values deviated more significantly from the random and complete catalog results obtained previously. At this point it is also of interest to compute the value of $\langle T_c \rangle$ explained in the Methodology section.

Figure 9 shows the variation of $\langle T_c \rangle$, the k - M slope, and the b -value with time for each of the three seismic zones in northern Iran. The time-magnitude sequence is also included for reference. Note that the behavior of the k - M slope and the b -value is very similar along time for all three zones. This is consistent with the results presented before. We note that there seems to be a correlation between the behavior of the b -value in time with the occurrence of some of these larger events. In particular, some of the events in the figure seem to coincide with a drop in the b -value.

The decline of the b -value before large earthquakes has been studied in other regions before (e.g., Wyss et al., 2000; Wyss and Stefansson, 2006; Schorlemmer et al., 2005; Chan et al., 2012). In the context of the visibility graph analysis, Telesca et al. (2016) observed a decrease in $\langle T_c \rangle$ before the large earthquake of the western India earthquake sequence. We recognize, however, that the lack of larger ($M > 6$) events in our region of interest in the last decade prevents us from drawing a stronger conclusion on this regard.

CONCLUSIONS

We studied the seismicity of the three main seismic regions in northern Iran in the time period between January 2005 and December 2015 using an approach based on the visibility graph method. We tested the applicability of this method for the specific region of interest and in reference to previous results from similar studies. The results confirm previous observations about the correlation

280 that exists between the connectivity parameter k , the magnitude of the events in the sequence, the slope of this relationship or k - M
281 slope, and the b -value from the Gutenberg-Richter law. We obtained mathematical expressions for the region of interest as well
282 as for so-called universal data collected from this study and previous additional analysis for other regions as well as data from
283 experiments and found the relationships to have a good level of similarity. This is indicative of the general nature of the relationship
284 between the k - M slope and the b value. We also explored the potential relationships that can be drawn from a time-dependent
285 visibility graph analysis and the variation of the seismicity in the region of interest. We found there may be a potential relationship
286 between the the b value and the occurrence of earthquakes as well as with the graph's mean interval connectivity time parameter
287 $\langle T_c \rangle$, but additional research in regions with stronger events may be necessary before drawing stronger conclusions in this regard.
288 The method used here, nonetheless, seems to provide an alternative and interesting approach to the analysis of the seismicity of a
289 region.

290 DATA AND RESOURCES

291 Data used to compile the seismic catalog employed in the analysis was obtained using the Web browser search application from
292 the International Institute of Earthquake Engineering and Seismology, IIEES (<http://www.iiees.ac.ir/en/eqcatalog/>, last accessed
293 September 2016). The raw versions of figures were prepared using MATLAB®, release 13b; and the Generic Mapping Tools,
294 version 5.1 (<http://gmt.soest.hawaii.edu>; Wessel et al., 2013). Final versions of figures were prepared using Adobe® Illustrator®.
295

ACKNOWLEDGMENTS

297 This research was possible thanks to support from the Center for Earthquake Research and Information (CERI) at the University of
298 Memphis. CERI is designated as a Center of Excellence by the Tennessee Board of Regents and is funded in part by the State of
299 Tennessee under State Sunset Laws (SB 1510 and HB 1608, 2015–2016).

REFERENCES

- Ahmadlou, M., Adeli, H., and Adeli, A. (2010). New diagnostic EEG markers of the Alzheimer's disease using visibility graph. *Journal of Neural Transmission*, 117(9):1099–1109, doi [10.1007/s00702-010-0450-3](https://doi.org/10.1007/s00702-010-0450-3).
- Aki, K. (1965). Maximum likelihood estimate of b in the formula $\log N = a - bM$ and its confidence limits. *Bull. Earthq. Res. Inst. Tokyo Univ.*, 43:237–239.
- Ambraseys, N. N. and Melville, C. P. (1982). *A history of Persian earthquakes*. Cambridge University Press, Cambridge, United Kingdom.
- Berberian, M. (1981). Active faulting and tectonics of Iran. In Gupta, H. K. and Delany, F. M., editors, *Zagros Hindu Kush Himalaya Geodynamic Evolution*. American Geophysical Union, Washington, D. C.
- Berberian, M. and Arshadi, S. (1976). On the evidence of the youngest activity of the North Tabriz Fault and the seismicity of Tabriz city. *Geol. Surv. Iran Rep.*, 39:397–418.
- Berberian, M. and Yeats, R. S. (1999). Patterns of historical earthquake rupture in the Iranian Plateau. *Bulletin of the Seismological Society of America*, 89(1):120–139.
- Berberian, M. and Yeats, R. S. (2001). Contribution of archaeological data to studies of earthquake history in the Iranian Plateau. *Journal of Structural Geology*, 23(2):563–584, doi [10.1016/S0191-8141\(00\)00115-2](https://doi.org/10.1016/S0191-8141(00)00115-2).
- Chan, C.-H., Wu, Y.-M., Tseng, T.-L., Lin, T.-L., and Chen, C.-C. (2012). Spatial and temporal evolution of b-values before large earthquakes in taiwan. *Tectonophysics*, 532:215–222.
- Deniz, A. and Yucemen, M. S. (2010). Magnitude conversion problem for the Turkish earthquake data. *Natural Hazards*, 55(2):333–352, doi [10.1007/s11069-010-9531-8](https://doi.org/10.1007/s11069-010-9531-8).
- Elsner, J. B., Jagger, T. H., and Fogarty, E. A. (2009). Visibility network of United States hurricanes. *Geophysical Research Letters*, 36(16):L16702, doi [10.1029/2009GL039129](https://doi.org/10.1029/2009GL039129).
- Gardner, J. and Knopoff, L. (1974). Is the sequence of earthquakes in Southern California, with aftershocks removed, Poissonian. *Bulletin of the Seismological Society of America*, 64(5):1363–1367.
- Ghafory-Ashtiani, M. (1999). Rescue operation and reconstruction of recent earthquakes in Iran. *Disaster Prevention and Management: An International Journal*, 8(1):5–20, doi [10.1108/09653569910258174](https://doi.org/10.1108/09653569910258174).
- Gutenberg, B. and Richter, C. F. (1944). Frequency of earthquakes in California. *Bulletin of the Seismological Society of America*, 34(4):185–188.
- Huang, H.-P. and Chung, S.-Y. (2004). Dynamic visibility graph for path planning. In *Proceedings of the IEEE/RSJ International Conference on Intelligent Robots and Systems (IROS)*, volume 3, pages 2813–2818.
- Jones, H. (1834). *An Account of the Transactions of His Majesty's Mission to the Court of Persia: In the Years 1807-11*, volume 1. James Bohn.
- Karimiparidari, S., Zaré, M., Memarian, H., and Kijko, A. (2013). Iranian earthquakes, a uniform catalog with moment magnitudes. *Journal of seismology*, 17(3):897–911, doi [10.1007/s10950-013-9360-9](https://doi.org/10.1007/s10950-013-9360-9).
- Khoshnevis, N., Taborda, R., Azizzadeh-Roodpish, S., and Cramer, C. H. (2016). Seismic hazard estimation of northern iran using smoothed seismicity. *Journal of Seismology*. Submitted for publication.
- Lacasa, L., Luque, B., Ballesteros, F., Luque, J., and Nuno, J. C. (2008). From time series to complex networks: The visibility graph. *Proceedings of the National Academy of Sciences*, 105(13):4972–4975, doi [10.1073/pnas.0709247105](https://doi.org/10.1073/pnas.0709247105).
- Long, Y. (2013). Visibility graph network analysis of gold price time series. *Physica A: Statistical Mechanics and its Applications*, 392(16):3374–3384, doi [10.1016/j.physa.2013.03.063](https://doi.org/10.1016/j.physa.2013.03.063).

- 337 Lozano-Pérez, T. and Wesley, M. A. (1979). An algorithm for planning collision-free paths among polyhedral obstacles. *Communications of the*
338 *ACM*, 22(10):560–570, doi [10.1145/359156.359164](https://doi.org/10.1145/359156.359164).
- 339 Mehrain, M. (1990). Reconnaissance report on the northern Iran earthquake of June 21, 1990. Technical Report NCEER-90-0017, National
340 Center for Earthquake Engineering Research (NCEER).
- 341 Mirzaei, N., Mengtan, G., and Yuntai, C. (1998). Seismic source regionalization for seismic zoning of Iran: Major seismotectonic provinces.
342 *Journal of Earthquake Prediction Research*, 7(4):465–495.
- 343 Nemati, M. (2015). Intermediate-term variations in 200 years seismicity of south of Iran. *Geomatics, Natural Hazards and Risk*, 7(3):1065–1080,
344 doi [10.1080/19475705.2015.1030785](https://doi.org/10.1080/19475705.2015.1030785).
- 345 Nowroozi, A. A. (1976). Seismotectonic provinces of Iran. *Bulletin of the Seismological Society of America*, 66(4):1249–1276.
- 346 Oommen, B., Iyengar, S., Rao, N., and Kashyap, R. (1987). Robot navigation in unknown terrains using learned visibility graphs. Part I: The
347 disjoint convex obstacle case. *IEEE Journal on Robotics and Automation*, 3(6):672–681, doi [10.1109/JRA.1987.1087133](https://doi.org/10.1109/JRA.1987.1087133).
- 348 Phillips, J. D., Schwanghart, W., and Heckmann, T. (2015). Graph theory in the geosciences. *Earth-Science Reviews*, 143:147–160, doi
349 [10.1016/j.earscirev.2015.02.002](https://doi.org/10.1016/j.earscirev.2015.02.002).
- 350 Raman, S. (2010). Designing a liveable compact city: Physical forms of city and social life in urban neighbourhoods. *Built Environment*,
351 36(1):63–80, doi [10.2148/benv.36.1.63](https://doi.org/10.2148/benv.36.1.63).
- 352 Razzaghi, M. S. and Ghafory-Ashtiani, M. (2012). A preliminary reconnaissance report on August 11th 2012, Varzaghan-Ahar twin earth-
353 quakes in NW of Iran. Technical report, International Association of Seismology and Physics of the Earth’s Interior, and Iranian Earthquake
354 Engineering Association.
- 355 Schorlemmer, D., Wiemer, S., and Wyss, M. (2005). Variations in earthquake-size distribution across different stress regimes. *Nature*,
356 437(7058):539–542, doi [10.1038/nature04094](https://doi.org/10.1038/nature04094).
- 357 Skiena, S. S. (2008). *The Algorithm Design Manual*. Springer, London, second edition.
- 358 Stocklin, J. (1968). Structural history and tectonics of Iran: A review. *AAPG Bulletin*, 52(7):1229–1258.
- 359 Takin, M. (1972). Iranian geology and continental drift in the Middle East. *Nature*, 235(5334):147–150, doi [10.1038/235147a0](https://doi.org/10.1038/235147a0).
- 360 Tavakoli, B. and Ghafory-Ashtiani, M. (1999). Seismic hazard assessment of Iran. *Annals of Geophysics*, 42(6):1013–1021, doi [10.4401/ag-3781](https://doi.org/10.4401/ag-3781).
- 361 Telesca, L. and Lovallo, M. (2012). Analysis of seismic sequences by using the method of visibility graph. *EPL (Europhysics Letters)*,
362 97(5):50002, doi [10.1209/0295-5075/97/50002](https://doi.org/10.1209/0295-5075/97/50002).
- 363 Telesca, L., Lovallo, M., Aggarwal, S., Khan, P., and Rastogi, B. (2016). Visibility graph analysis of the 2003–2012 earthquake sequence in the
364 Kachchh region of western India. *Pure and Applied Geophysics*, 173(1):125–132, doi [10.1007/s00024-015-1034-9](https://doi.org/10.1007/s00024-015-1034-9).
- 365 Telesca, L., Lovallo, M., and Pierini, J. O. (2012). Visibility graph approach to the analysis of ocean tidal records. *Chaos, Solitons & Fractals*,
366 45(9):1086–1091, doi [10.1016/j.chaos.2012.06.003](https://doi.org/10.1016/j.chaos.2012.06.003).
- 367 Telesca, L., Lovallo, M., Ramirez-Rojas, A., and Flores-Marquez, L. (2013). Investigating the time dynamics of seismicity by using the visibility
368 graph approach: Application to seismicity of Mexican subduction zone. *Physica A: Statistical Mechanics and its Applications*, 392(24):6571–
369 6577, doi [10.1016/j.physa.2013.08.078](https://doi.org/10.1016/j.physa.2013.08.078).
- 370 Telesca, L., Lovallo, M., Ramirez-Rojas, A., and Flores-Marquez, L. (2014a). Relationship between the frequency magnitude distribution and the
371 visibility graph in the synthetic seismicity generated by a simple stick-slip system with asperities. *PLOS ONE*, 9(8):e106233, doi [10.1371/journal.pone.0106233](https://doi.org/10.1371/journal.pone.0106233).

- 373 Telesca, L., Lovallo, M., and Toth, L. (2014b). Visibility graph analysis of 2002–2011 Pannonian seismicity. *Physica A: Statistical Mechanics
374 and its Applications*, 416:219–224, doi [10.1016/j.physa.2014.08.048](https://doi.org/10.1016/j.physa.2014.08.048).
- 375 Trifonov, V. G. (1978). Late quaternary tectonic movements of Western and Central Asia. *Geological Society of America Bulletin*, 89(7):1059–
376 1072, doi [10.1130/0016-7606\(1978\)89<1059:LQTMOW>2.0.CO;2](https://doi.org/10.1130/0016-7606(1978)89<1059:LQTMOW>2.0.CO;2).
- 377 Varoudis, T. and Psarra, S. (2014). Beyond two dimensions: Architecture through three dimensional visibility graph analysis. *The Journal of
378 Space Syntax*, 5(1):91–108.
- 379 Wang, N., Li, D., and Wang, Q. (2012). Visibility graph analysis on quarterly macroeconomic series of China based on complex network theory.
380 *Physica A: Statistical Mechanics and its Applications*, 391(24):6543–6555, doi [10.1016/j.physa.2012.07.054](https://doi.org/10.1016/j.physa.2012.07.054).
- 381 Wessel, P., Smith, W. H. F., Scharroo, R., Luis, J., and Wobbe, F. (2013). Generic mapping tools: Improved version released. *Eos, Transactions
382 American Geophysical Union*, 94(45):409–410, doi [10.1002/2013EO450001](https://doi.org/10.1002/2013EO450001).
- 383 Wiemer, S. (2001). A software package to analyze seismicity: ZMAP. *Seismological Research Letters*, 72(3):373–382, doi [10.1785/gssrl.72.3.373](https://doi.org/10.1785/gssrl.72.3.373).
- 384 Wiemer, S. and Wyss, M. (2000). Minimum magnitude of completeness in earthquake catalogs: examples from Alaska, the Western United
385 States, and Japan. *Bulletin of the Seismological Society of America*, 90(4):859–869, doi [10.1785/0119990114](https://doi.org/10.1785/0119990114).
- 386 Wyss, M., Schorlemmer, D., and Wiemer, S. (2000). Mapping asperities by minima of local recurrence time: San Jacinto-Elsinore fault zones.
387 *Journal of Geophysical Research: Solid Earth*, 105(B4):7829–7844, doi [10.1029/1999JB900347](https://doi.org/10.1029/1999JB900347).
- 388 Wyss, M. and Stefansson, R. (2006). Nucleation points of recent mainshocks in southern Iceland, mapped by *b*-values. *Bulletin of the Seismological
389 Society of America*, 96(2):599–608, doi [10.1785/0120040056](https://doi.org/10.1785/0120040056).
- 390 Yang, Y., Wang, J., Yang, H., and Mang, J. (2009). Visibility graph approach to exchange rate series. *Physica A: Statistical Mechanics and its
391 Applications*, 388(20):4431–4437, doi [10.1016/j.physa.2009.07.016](https://doi.org/10.1016/j.physa.2009.07.016).
- 392 Zare, M., Amini, H., Yazdi, P., Sesetyan, K., Demircioglu, M. B., Kalafat, D., Erdik, M., Giardini, D., Khan, M. A., and Tsereteli, N. (2014).
393 Recent developments of the middle east catalog. *Journal of Seismology*, 18(4):749–772, doi [10.1007/s10950-014-9444-1](https://doi.org/10.1007/s10950-014-9444-1).

Table 1: Total and declustered number of earthquakes and seismic parameters M_c and b for the three seismic zones of northern Iran.

Region	Total Num. of Events	Declus. Num. of Events	M_c	b -value
Azerbaijan	271	93	3.5	1.02
Alborz	1262	794	2.6	0.77
Kopeh Dagh	399	282	2.6	0.58

Figure Captions

- 395 **Figure 1.** Illustration of the visibility graph method, as applied to a subset of events in a window of the magnitude-
 396 time series of the north Iranian seismic region of Kopeh Dagh. The events are identified by vertical thick
 397 lines (or sticks) on the horizontal time axis with size equal to the magnitude as indicated by the labels
 398 at the bottom of each stick. These sticks are considered to be the obstacles in the time-magnitude space
 399 where the graph resides. The visibility graph is composed by the nodes, represented with circles at the tip
 400 of each event stick, and the edges or links connecting them. The values inside each node correspond to
 401 the connectivity degree, k . This value indicates the number straight lines that can be draw between two
 402 (mutually visible) nodes without intersecting any obstacle (event stick). The values and time ranges shown
 403 at the top correspond to the time difference between events visible by the last event. These times are given
 404 in minutes and correspond to individual T_c values. The mean $\langle T_c^e \rangle$ value associated with this event is also
 405 shown at the top right. The mean value of all $\langle T_c^e \rangle$ for the events in the graph is the window mean interval
 406 connectivity time, $\langle T_c^e \rangle$. The color version of this figure is available only in the electronic edition.
- 407 **Figure 2.** Region of interest, highlighting the seismic zones that are the focus of this study: Azerbaijan, Alborz,
 408 and Kopeh Dagh. The top-right location-map shows Iran and the selected area with respect to neighboring
 409 countries. The solid dark lines show the boundaries of the additional Zagros and Central-East seismic zones.
 410 This zonation follows the division proposed by Mirzaei et al. (1998) and later modified by Karimiparidari
 411 et al. (2013). The background shows fault lines and the shaded relief. The color version of this figure is
 412 available only in the electronic edition.
- 413 **Figure 3.** Declustered instrumental seismicity of northern Iran for the 2005–2015 period, considering only the events
 414 in the seismic zones of interest, namely Azerbaijan, Alborz, and Kopeh Dagh. The size of symbols are
 415 proportional to the magnitude of the events, as indicated by the artificial scale shown on the right. The
 416 background shows fault lines and the shaded relief. The color version of this figure is available only in the
 417 electronic edition.
- 418 **Figure 4.** Completeness magnitude goodness-of-fit test (GFT) results and selected M_c values for the three tectonic
 419 seismic regions in northern Iran as evaluated from the time-magnitude sequence of earthquakes during
 420 the 2005–2015 period. The symbols indicate the computed GFT values as function of the earthquake
 421 magnitude. The horizontal dashed line indicates the desired threshold for the GFT value at 90 percent. The
 422 vertical dashed lines and solid symbols indicate the selected completeness magnitude for each region. The
 423 color version of this figure is available only in the electronic edition.

- 424 **Figure 5.** Time-magnitude sequences for the northern Iran seismic zones of Azerbaijan, Alborz and Kopeh Dagh,
 425 during the period between 1 January 2005 and 31 December 2015. The event occurrences are represented by
 426 vertical bars or sticks of length equal to the M_w magnitude of each earthquake. These sequences correspond
 427 to the declustered catalog but in each case we consider only events with $M_w \geq M_c$. As shown in Fig. 1, the
 428 dots at the top of each stick represent the nodes of the visibility graphs. The edges or links are omitted for
 429 visual convenience. Highlighted in the figure are the largest events in each sub-catalog, namely the 2012
 430 M_w 6.4 East Azerbaijan, 2010 M_w 5.8 Damghan, and 2012 M_w 5.4 Neyshabur earthquakes. The color
 431 version of this figure is available only in the electronic edition.
- 432 **Figure 6.** Scattered distribution of events in the magnitude-connectivity degree plane and linear regressions obtained
 433 for the k - M relationships for the three seismic regions in northern Iran. The value next to each of regression
 434 line corresponds to the slope of the line, which is referred here as the k - M slope. The color version of this
 435 figure is available only in the electronic edition.
- 436 **Figure 7.** Correlation between k - M slope and b -value as drawn from the results of the present study for the region
 437 of northern Iranian and three other previous studies, including analysis of the Mexican subduction zone
 438 (Telesca et al., 2013), the Pannonian seismic zone (Telesca et al., 2014b), and results from two experiments
 439 (Telesca et al., 2014a). The lines represent linear regressions obtained to fit the different data points, consid-
 440 ering different combinations. The values of the correlation coefficient, R , are indicated for each regression
 441 line. The color version of this figure is available only in the electronic edition.
- 442 **Figure 8.** (a) Correlation between k - M slope and b -values for 200 random sequences extracted from the initial cat-
 443 alogs of the three northern Iranian seismic regions considered in this study (scattered symbols), including
 444 the mean values (empty symbols with thick border) and the data points obtained from the analysis of the
 445 complete catalog (solid symbols), along with the linear regressions of each sample as indicated in the leg-
 446 end. (b) Mean, ± 1 standard deviation, and coefficient of variation (in percent) for the k - M slope values of
 447 the three seismic zones in northern Iran. (c) Same as part (b), but corresponding to the b -value. The color
 448 version of this figure is available only in the electronic edition.
- 449 **Figure 9.** Variation of $\langle T_c \rangle$, k - M slope and b -value as with respect to time for three seismic zones for a moving win-
 450 dow analysis of the visibility graphs of sub-sequences of 20 consecutive events, along with the magnitude
 451 of events in the 2005–2015 period. Black triangles indicate the occurrence of major earthquakes in each
 452 of the regions, with the corresponding magnitude at the top of each symbol. In the middle frame of each
 453 region, the dashed line corresponds to the k - M values, whereas the continuous plot shows the variation of
 454 the b -value. The color version of this figure is available only in the electronic edition.

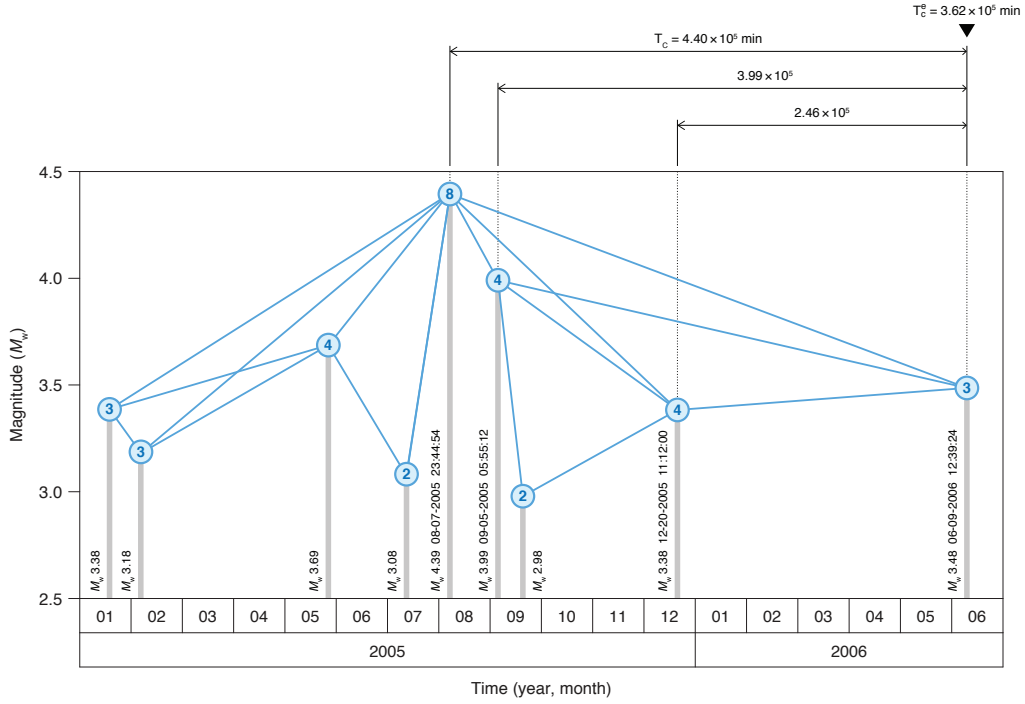


Figure 1: Illustration of the visibility graph method, as applied to a subset of events in a window of the magnitude-time series of the north Iranian seismic region of Kopeh Dagh. The events are identified by vertical thick lines (or sticks) on the horizontal time axis with size equal to the magnitude as indicated by the labels at the bottom of each stick. These sticks are considered to be the obstacles in the time-magnitude space where the graph resides. The visibility graph is composed by the nodes, represented with circles at the tip of each event stick, and the edges or links connecting them. The values inside each node correspond to the connectivity degree, k . This value indicates the number straight lines that can be drawn between two (mutually visible) nodes without intersecting any obstacle (event stick). The values and time ranges shown at the top correspond to the time difference between events visible by the last event. These times are given in minutes and correspond to individual T_c values. The mean $\langle T_c^e \rangle$ value associated with this event is also shown at the top right. The mean value of all $\langle T_c^e \rangle$ for the events in the graph is the window mean interval connectivity time, $\langle T_c^e \rangle$. The color version of this figure is available only in the electronic edition.

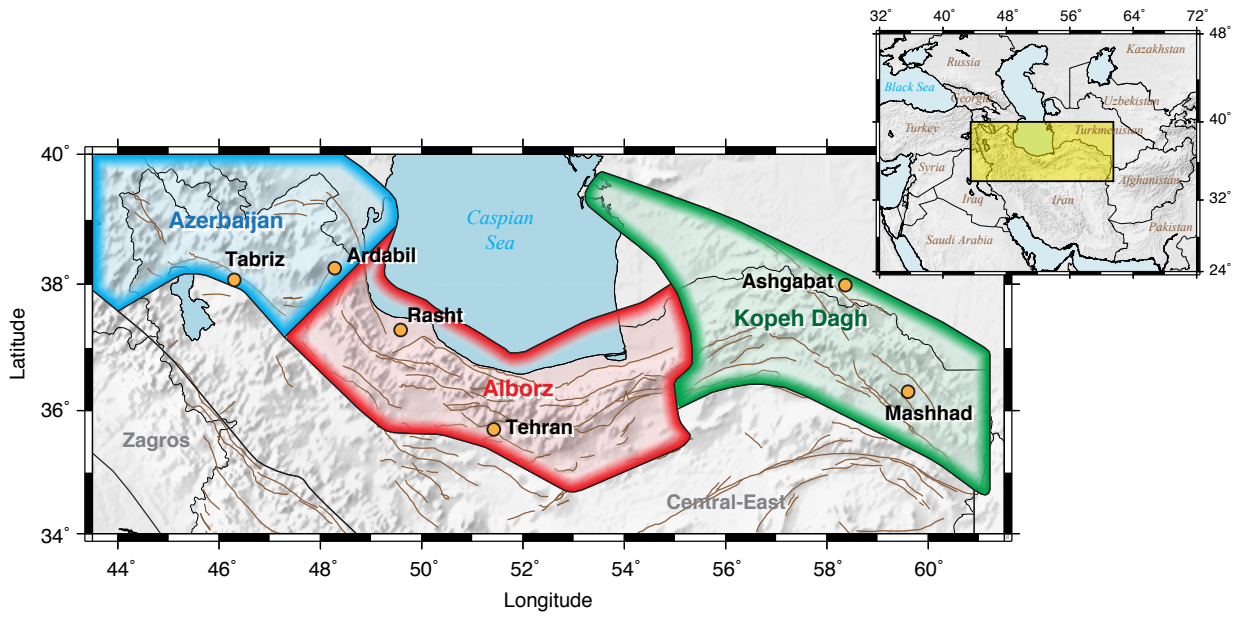


Figure 2: Region of interest, highlighting the seismic zones that are the focus of this study: Azerbaijan, Alborz, and Kopeh Dagh. The top-right location-map shows Iran and the selected area with respect to neighboring countries. The solid dark lines show the boundaries of the additional Zagros and Central-East seismic zones. This zonation follows the division proposed by [Mirzaei et al. \(1998\)](#) and later modified by [Karimiparidari et al. \(2013\)](#). The background shows fault lines and the shaded relief. The color version of this figure is available only in the electronic edition.

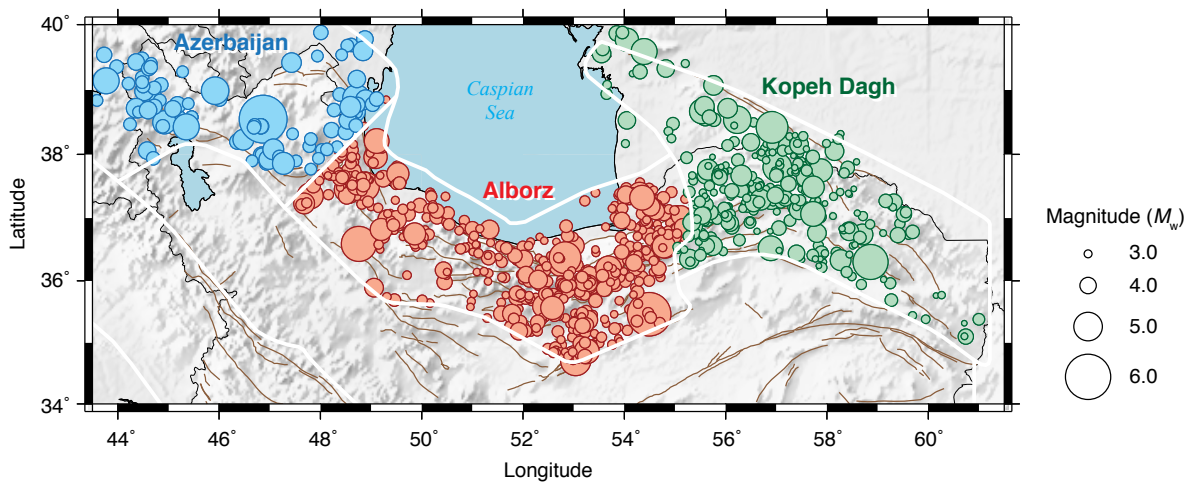


Figure 3: Declustered instrumental seismicity of northern Iran for the 2005–2015 period, considering only the events in the seismic zones of interest, namely Azerbaijan, Alborz, and Kopeh Dagh. The size of symbols are proportional to the magnitude of the events, as indicated by the artificial scale shown on the right. The background shows fault lines and the shaded relief. The color version of this figure is available only in the electronic edition.

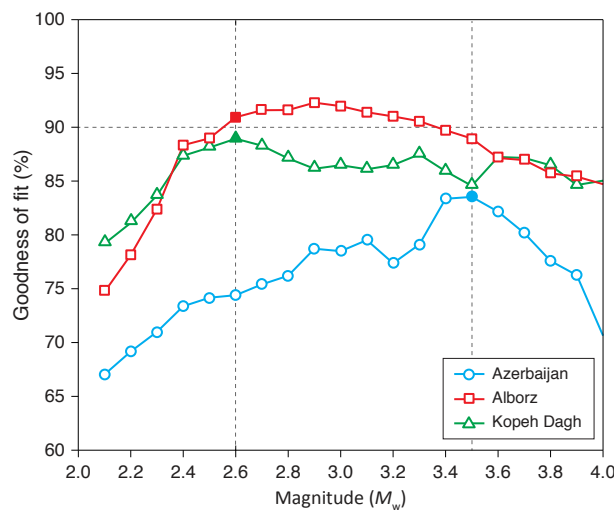


Figure 4: Completeness magnitude goodness-of-fit test (GFT) results and selected M_c values for the three tectonic seismic regions in northern Iran as evaluated from the time-magnitude sequence of earthquakes during the 2005–2015 period. The symbols indicate the computed GFT values as function of the earthquake magnitude. The horizontal dashed line indicates the desired threshold for the GFT value at 90 percent. The vertical dashed lines and solid symbols indicate the selected completeness magnitude for each region. The color version of this figure is available only in the electronic edition.

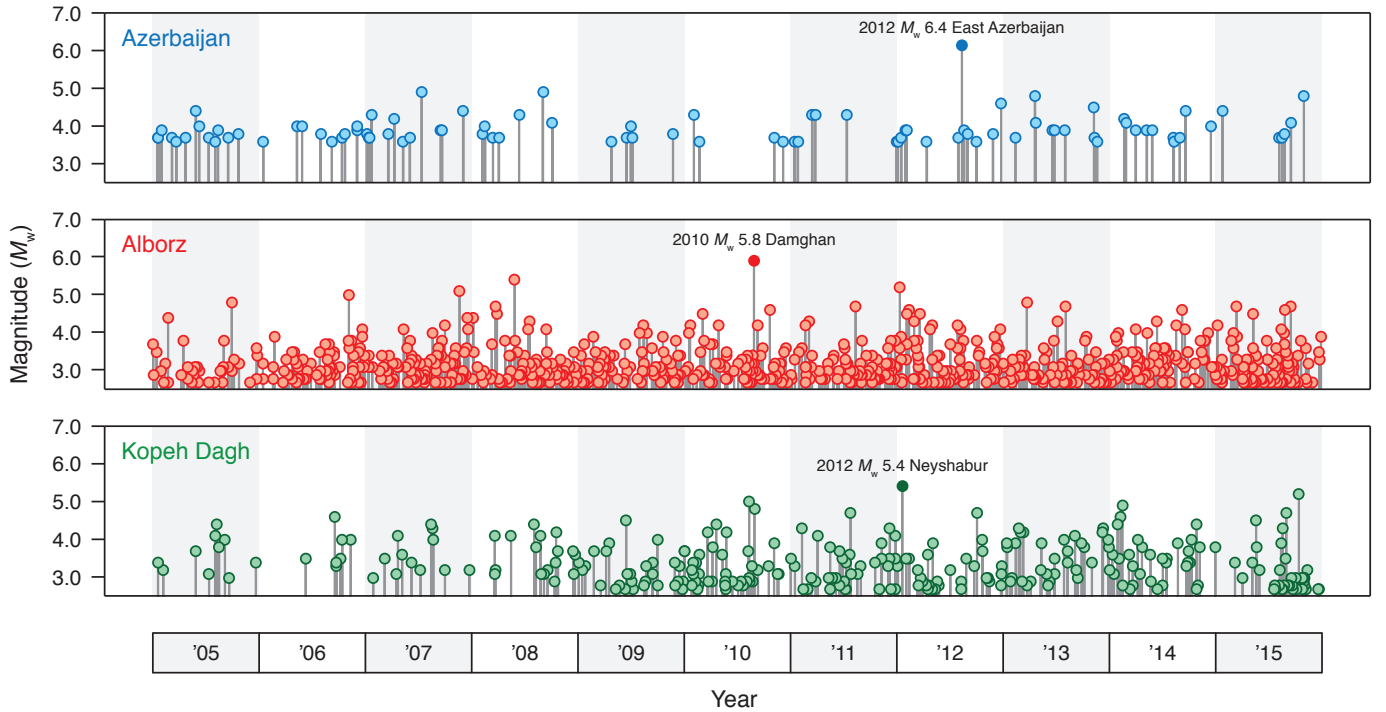


Figure 5: Time-magnitude sequences for the northern Iran seismic zones of Azerbaijan, Alborz and Kopeh Dagh, during the period between 1 January 2005 and 31 December 2015. The event occurrences are represented by vertical bars or sticks of length equal to the M_w magnitude of each earthquake. These sequences correspond to the declustered catalog but in each case we consider only events with $M_w \geq M_c$. As shown in Fig. 1, the dots at the top of each stick represent the nodes of the visibility graphs. The edges or links are omitted for visual convenience. Highlighted in the figure are the largest events in each sub-catalog, namely the 2012 M_w 6.4 East Azerbaijan, 2010 M_w 5.8 Damghan, and 2012 M_w 5.4 Neyshabur earthquakes. The color version of this figure is available only in the electronic edition.

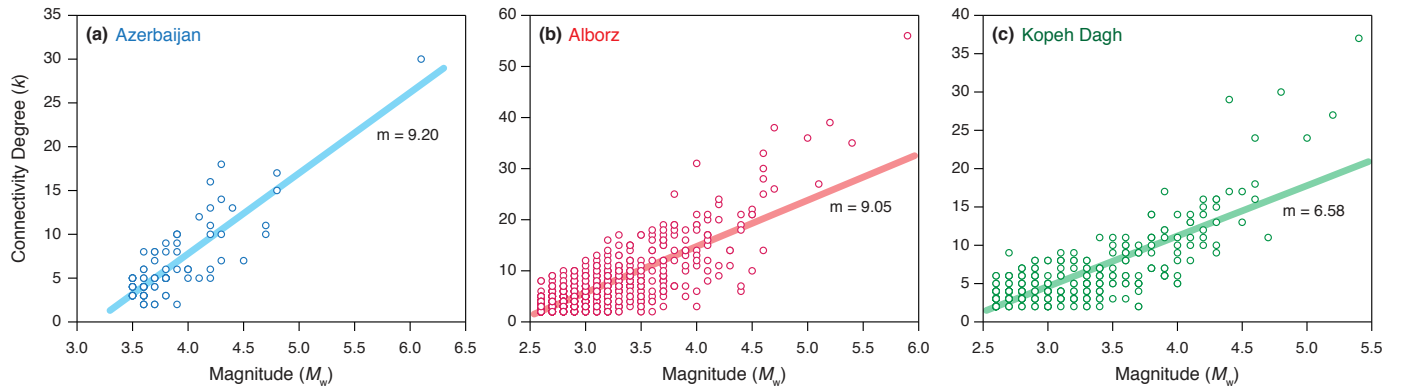


Figure 6: Scattered distribution of events in the magnitude-connectivity degree plane and linear regressions obtained for the k - M relationships for the three seismic regions in northern Iran. The value next to each of regression line corresponds to the slope of the line, which is referred here as the k - M slope. The color version of this figure is available only in the electronic edition.

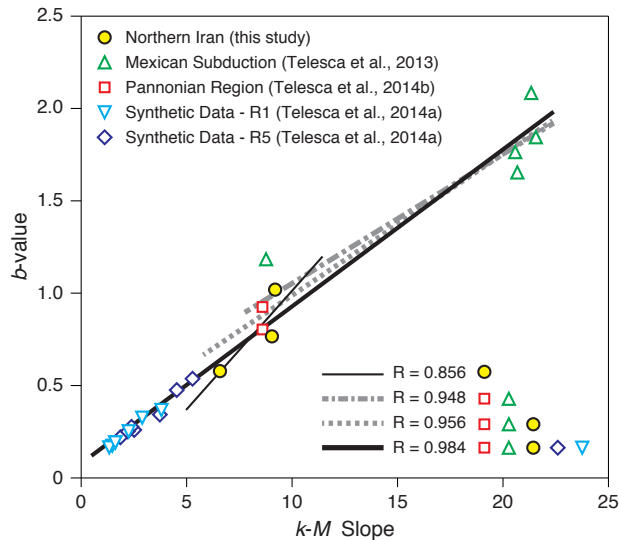


Figure 7: Correlation between k - M slope and b -value as drawn from the results of the present study for the region of northern Iranian and three other previous studies, including analysis of the Mexican subduction zone (Telesca et al., 2013), the Pannonian seismic zone (Telesca et al., 2014b), and results from two experiments (Telesca et al., 2014a). The lines represent linear regressions obtained to fit the different data points, considering different combinations. The values of the correlation coefficient, R , are indicated for each regression line. The color version of this figure is available only in the electronic edition.

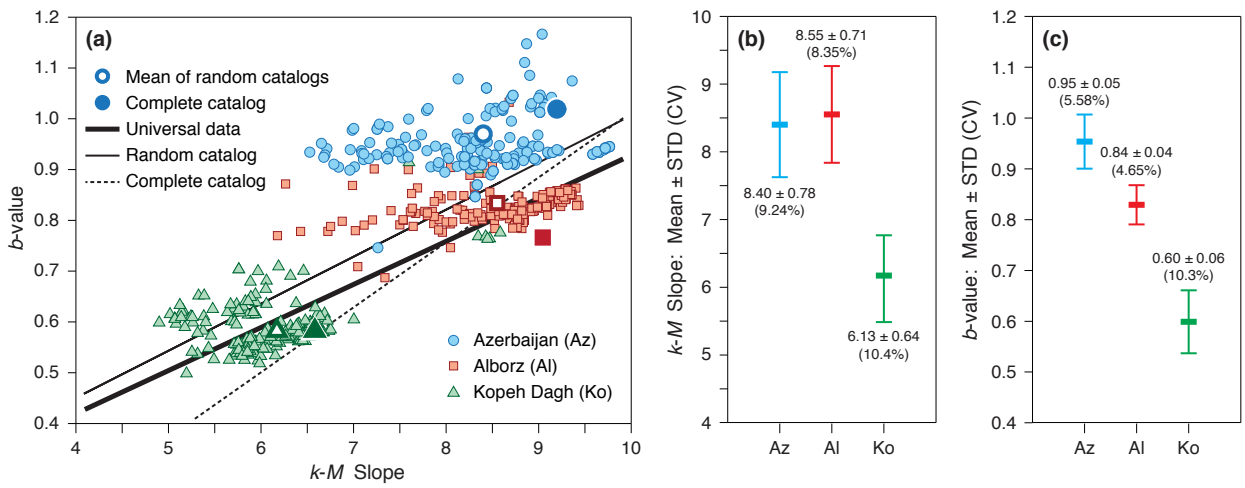


Figure 8: (a) Correlation between $k\text{-}M$ slope and b -values for 200 random sequences extracted from the initial catalogs of the three northern Iranian seismic regions considered in this study (scattered symbols), including the mean values (empty symbols with thick border) and the data points obtained from the analysis of the complete catalog (solid symbols), along with the linear regressions of each sample as indicated in the legend. (b) Mean, ± 1 standard deviation, and coefficient of variation (in percent) for the $k\text{-}M$ slope values of the three seismic zones in northern Iran. (c) Same as part (b), but corresponding to the b -value. The color version of this figure is available only in the electronic edition.

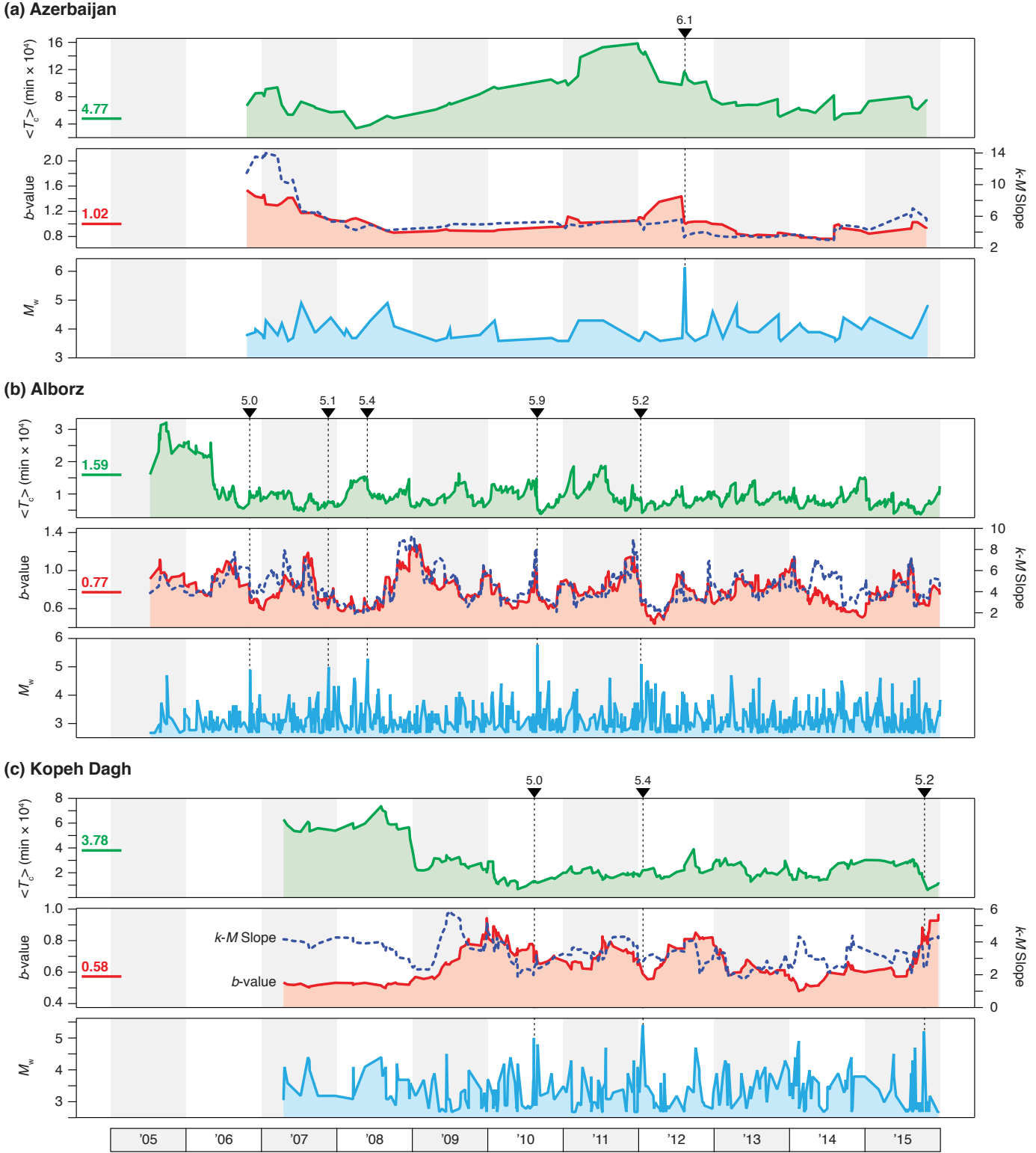


Figure 9: Variation of $\langle T_c \rangle$, k - M slope and b -value as with respect to time for three seismic zones for a moving window analysis of the visibility graphs of sub-sequences of 20 consecutive events, along with the magnitude of events in the 2005–2015 period. Black triangles indicate the occurrence of major earthquakes in each of the regions, with the corresponding magnitude at the top of each symbol. In the middle frame of each region, the dashed line corresponds to the k - M values, whereas the continuous plot shows the variation of the b -value. The color version of this figure is available only in the electronic edition.